Hindawi
Journal of Mathematics
Volume 2023, Article ID 3099858, 15 pages
https://doi.org/10.1155/2023/3099858

Research Article

Analysis of a Two-Phase MHD Free Convection Generalized Water–Ethylene Glycol (50 : 50) Dusty Brinkman-Type Nanofluid Pass through Microchannel

Dolat Khan,[1] **Musawa Yahya Almusawa**,[2] **Waleed Hamali**,[2] **and M. Ali Akbar**[3]

[1]*Faculty of Science, King Mongkut's University of Technology Thonburi (KMUTT), 126 Pracha Uthit Rd., Bang Mod, Thung Khru, Bangkok 10140, Thailand*
[2]*Department of Mathematics, Faculty of Science, Jazan University, Jizan, Saudi Arabia*
[3]*Department of Applied Mathematics, University of Rajshahi Bangladesh, Rajshahi, Bangladesh*

Correspondence should be addressed to M. Ali Akbar; ali.akbar@ru.ac.bd

Received 28 October 2022; Revised 30 November 2022; Accepted 18 April 2023; Published 9 May 2023

Academic Editor: M. M. Bhatti

The water–ethylene glycol (50 : 50) nanofluid has applications in the manufacture of polyester as a raw agent, air conditioning systems, antifreeze formulation, dehydrating agents in the gas industry, a precursor in the plastic industry, and convective heat transfer. These developments in nanotechnology and nanoscience have caught the interest of several researchers. Because it keeps machines and engines cool by reducing friction between their different parts, grease is a vital part of many machinery and engines. Also, due to the extensive use of fractional derivatives, this work seeks to evaluate the combined impacts of free convection flow and heat transfer, magnetic field, and Brinkman-type water–ethylene glycol (50 : 50) dusty nanofluid among microchannel. The flow that the buoyant force provides helps to carry heat naturally via convection. While the left plate moves at a consistent velocity and the right plate stays stationary, the fluid is also evenly dispersed with all dust particles that have a spherical form. Partial differential equations (PDE) are used to present the mathematical modeling. The resultant PDEs are generalized by utilizing the Caputo–Fabrizio fractional derivative. The problem's closed-form solution is produced by combining a Laplace transformation with a finite sine Fourier transformation. It has also been studied that temperature, Brinkman nanofluid, and dust particle velocity relate to a variety of other factors, such as the magnetic parameter, Grashof number, dusty fluid parameter, and volume friction parameter. The graphical outcomes for the dusty fluid, Brinkman nanofluid, and temperature profiles are plotted using Mathcad-15. The Brinkman nanofluid and dusty fluid behave similarly for a variety of embedded factors. It is found that compared to the traditional one, the fractional dusty nanofluid model displays more realistic characteristics. The addition of nanoparticles in water–ethylene glycol (50 : 50) dusty nanofluid enhances the rate of heat transfer up to 41.04478% by increasing their volume fractional.

1. Introduction

Materials with a size of 100 nanometers or less are known as nanomaterials, and the technology used to create them is referred to as nanotechnology. When classifying nanomaterials into one of four classes, attention is given to both the structure and the properties of the materials [1]. The first person's to look at the terminology used with nanofluids were Choi and Eastman [2]. To describe fluids containing particles with a diameter of less than 100 nanometers, he coined the term "nanofluid." Outline the justification for why nanoscale particles are preferred over microscale particles in many applications [3]. When comparing nanoparticles to microparticles, significant increases in thermophysical properties have been seen. Nanofluids may be used in several ways, such as improving the efficiency of diesel generators, cooling air conditioning systems, and cooling power plants [4]. Rehman et al. [5] analyzed the MHD flow of carbon in micropolar nanofluid in rotating frame geometry in addition to convective heat transfer.

Additionally, Ijaz Khan et al. [6] reported the relevant issues in optimizing entropy formation in nanomaterial flows with mixed convection. While the mixed convection flow of a tangent hyperbolic nanofluid was reported by Khan et al. [7]. To get a more realistic study Khan et al. [8] investigated the fractional model in the drilling process based on hybrid nanofluids with heat generation and porous medium. Furthermore, the growth of nanomaterials has made it possible to produce nanoparticles (also known as nanocomposites). Many researchers have lately focused on the properties of hybrid nanofluids, as mentioned by Leong et al. [9]. Khan et al. [10] present their analysis and evaluation of the joint Sumudu and Laplace transform for the MHD unsteady flow of hybrid nanofluid in a rotating frame. In order to represent and solve fractional differential equations for heat transportation in nanofluids, Saqib et al. [11] investigated the application of integral transforms.

Fractional calculus has useful applications in many areas of engineering and research, including viscoelasticity, including electromagnetics, fluid mechanics, biological population models, electrochemistry, signals processing, and optics. In order to solve various physical and natural issues that the conventional derivative cannot adequately represent, fractional calculus is applied, as shown in Ross [12]. Fractional derivatives have drawn considerable interest from scientists during the past 30 years. In response, numerous researchers have proposed different ways of defining fractional derivatives. In the 18^{th} century, Riemann–Liouville [13] became the most commonly used definition. The R-L concept of the fractional derivative has been faithfully reproduced in many physical systems, but it is only useable because of two key features. The Caputo fractional derivative has been extensively studied in the domains of chemistry, economics, physics, and other physical concerns. Exploration of diffusion, signal processing, image processing, damping, pharmacokinetics, material mechanics, and bioengineering processes are all conceivable using CFD [14–16]. To address concerns with the R-L formulation, CFD [17], a modified version of fractional calculus, was created. Yet because the CFD kernel has a singularity, it cannot be used to correctly describe materials with large heterogeneities [18]. To address this problem, a new definition with a nonsingular kernel has been proposed by Caputo–Fabrizio [19], and this novel idea has been applied in the research of several scholars [20–22]. Mohammadi [23] used fractional-time CF and Caputo derivatives to investigate the flow of couple stress fluids (CSF) between the two parallel plates. Research on the two-phase laminar flow of dusty fluid on elastic and stretching sheets was explored in detail by Mahanthesh [24].

Various branches of bioengineering, the pharmaceutical and chemical industries, mechanical engineering, nuclear power facilities, and so on all make use of fluids in some way. Scientists and researchers are increasingly focusing on fluids because of their widespread use, primarily discussing and debating their current and future capabilities, uses, and aims. Numerous mathematical models are put out in the literature to characterize the behavior of various fluids. The Brinkman model is among the most straightforward and widely used of these many options. A framework that may be used in huge, permeable regions was created by Brinkman's groundbreaking study [25]. He examined the behavior of fluid flow when dynamic viscosity develops on the surface of a dense cluster of small spheres using the Navier-Stoke equation.

The numerical technique was used by Liu et al. [26] to examine the continuous dependency of the Brinkman–Forchheimer fluid interacting with a Darcy fluid in a bounded region. Ramzan et al. [27] looked at the impacts of heat radiation and the Brinkman fluid on chemical reaction. It has been shown that heat radiation and mass Grashof numbers have an increasing influence on fluid velocity, but chemical reaction and magnetic field have a diminishing impact. Furthermore, the research conducted by Kumar et al. [28] focused on investigating the influence of diffusion and thermodynamics on the flow of a Brinkman-type nanofluid, which is both heat-radiating and chemically reactive. The flow was unsteady and hydromagnetic and occurred near an exponentially accelerated vertical plate through a porous medium. The temperature of the plate varied in an arbitrary ramped manner. Heat transfer, thermal radiation, chemical reactions, and magnetohydrodynamics were studied by Khan et al. [29] in the context of Brinkman fluid across a perpendicular plate. Dubey and Murthy [30] investigated how double-diffusive disease first manifests itself. The dust fluid through Brinkman porous media was reported by Kumar and Mohan [31].

The fluid containing the dust particles is used in a wide variety of mechanical procedures, including transport, the production of cement and steel, the removal of flying ash from thermal power plants, and the reduction of the unfavorable impacts of air conditioners. Numerous commercial applications exist for two-phase flows that include solid particles dispersed in nanofluids or hybrid nanofluids. Many scientists have been studying fluid flow with embedded dust particles lately. Experts are interested in dusty fluid models because they are two-phase systems. These occurrences occur in fluid flows containing dispersed solid particles. Both the analysis and the solution to the problem of the movement of dusty particles have been sped up. Saffman [32] is credited with initiating the study of laminar flow in dusty fluids. Specifically, Chakrabarti [33] looked at the behavior of a dusty gas as it approached the boundary layer. The motions of the dust fluid in densely interconnected dusty plasmas were investigated by Shukla and Stenflo [34]. We show that dusty plasmas with strong couplings may display zonal winds or vortex-like dust fluid movements when subjected to shear waves of sufficiently large amplitude.

In view of the above literature, the main objective of the present research is to investigate the water–ethylene glycol (50 : 50) dusty nanofluid using a newly created C-F time fractional derivative to give an exact solution. For the enhancement of heat transfer, cobalt ferrite, and magnetite nanoparticles are dispersed in the base fluid. The fluid is taken into a microchannel. In a two-phase flow model, fluid and dust particle equations are calculated separately. C-F time fractional derivative used to generalize the approach for more realistic. The exact

solution is obtained by coupling Laplace with the finite sine Fourier transform. Nusselt number and many embedded variables effects are graphically shown here using Mathcad-15.

2. Formulation and Solution

Assume that a water–ethylene glycol dusty nanofluid of the Brinkman type is flowing unsteadily and incompressibly between microchannels. The fluid as a whole evenly disperses a dust particle. The distance between two vertical, equivalent plates is represented by d, as shown in geometrical Figure 1. The fluid motion is along the x-direction. The uniform magnetic field is transverse to the dusty nanofluid. The left plate moves with $H(t)u_0$, while the right plate stays stationary. While denotes the temperature of the right plate by T_d, the left plate's temperature is $T_d + (T_w - T_d)At$.

As we have shown, there is a relationship between velocity and temperature [24]:

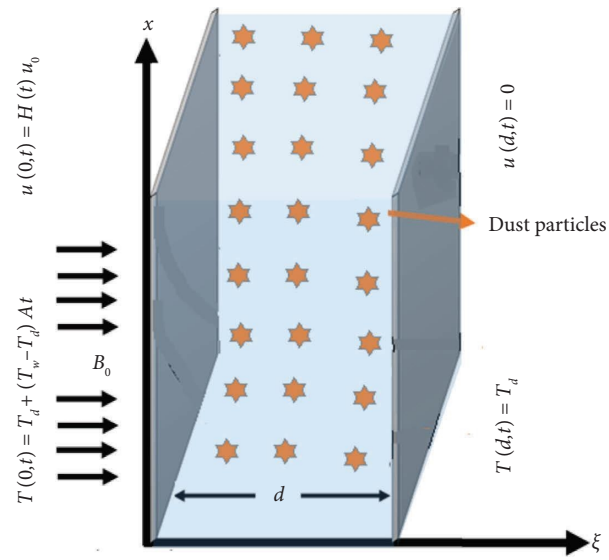

Figure 1: Problem geometric view.

$$\frac{\rho_{nf}\partial u(\xi,t)}{\partial t} + \beta\rho_{nf}u(\xi,t) = \frac{\mu_{nf}\partial^2 u(\xi,t)}{\partial\xi^2} + K_0N_0(v(\xi,t) - u(\xi,t)) + g(\beta_T\rho)_{nf}(T(\xi,t) - T_d) - B_0^2\sigma_{nf}u(\xi,t), \tag{1}$$

$$m\frac{\partial v(\xi,t)}{\partial t} = K_0(u(\xi,t) - v(\xi,t)), \tag{2}$$

$$\frac{\partial T(\xi,t)}{\partial t} = \frac{k_{nf}}{(\rho c_p)_{nf}}\frac{\partial^2 T(\xi,t)}{\partial\xi^2}. \tag{3}$$

Utilizing the conditions:

$$\left.\begin{aligned} &u(\xi,0) = v(\xi,0) = 0, u(0,t) = H(t)u_0 \\ &T(\xi,0) = T_d, u(d,t) = 0 \\ &T(0,t) = T_d + (T_w - T_d)At, T(d,t) = T_d \end{aligned}\right\}, \tag{4}$$

Expressions for $(\rho c_p)_{nf}, (\rho\beta_T)_{nf}, \mu_{nf}, \rho_{nf}, \sigma_{nf}, k_{nf}$ are given by [29]

$$\begin{aligned} \mu_{nf} &= \frac{1}{(1-\phi)^{2.5}}\mu_f, k_{nf} = k_f\left\{\frac{k_s + 2k_f - 2\phi(k_f - k_s)}{k_s + 2k_f + \phi(k_f - k_s)}\right\}, \\ \rho_{nf} &= \rho_f(1-\phi) + \rho_s\phi, \\ \sigma &= \frac{\sigma_f}{\sigma_s}, \\ \frac{\sigma_{nf}}{\sigma_f} &= 1 + \frac{3(\sigma-1)\phi}{(\sigma+2) - (\sigma-1)\phi}, \\ (\rho\beta_T)_{nf} &= (1-\phi)(\rho\beta_T)_f + \phi(\rho\beta_T)_s, \\ (\rho c_p)_{nf} &= (1-\phi)(\rho c_p)_f + \phi(\rho c_p)_s. \end{aligned} \tag{5}$$

We define the following dimensionless variables to create a dimensionless system of PDEs [24]:

$$\left.\begin{aligned} t = \frac{u_0}{d}t, u^* = \frac{u}{u_0}, y^* = \frac{1}{d}y, v^* = \frac{v}{u_0}, \theta^* = \frac{T - T_d}{T_d - T_d} \end{aligned}\right\}. \tag{6}$$

When we plug equation (6) into equations (1), (2), (3), and (4), we get the following dimensionless form:

$$\frac{\partial u(\xi,t)}{\partial t} = \frac{f_2}{f_1}\frac{\partial^2 u(\xi,t)}{\partial\xi^2} - \frac{1}{f_1}Hu(\xi,t) + \frac{1}{f_1}K(v(\xi,t) - u(\xi,t)) + \frac{f_3}{f_1}Gr\theta(\xi,t), \tag{7}$$

$$\frac{\partial v(\xi,t)}{\partial t} = P_m\{u(\xi,t) - v(\xi,t)\}, \tag{8}$$

$$\frac{\partial\theta(\xi,t)}{\partial t} = \frac{1}{\mathrm{Pr}}\frac{f_4}{f_5}\frac{\partial^2\theta(\xi,t)}{\partial\xi^2}. \tag{9}$$

This includes physical conditions that have no dimensions, such as [24]

$$\left.\begin{aligned} &u(y,0) = v(\xi,0) = 0, T(\xi,0) = 0 \\ &u(0,t) = H(t), T(0,t) = t, \\ &u(1,t) = 0 \quad T(1,t) = 0 \end{aligned}\right\}, \tag{10}$$

$$\begin{aligned} f_1 &= 1 - \phi + \phi\frac{\rho_s}{\rho_f}, \\ f_2 &= \frac{1}{(1-\phi)^{2.5}}, f_3 = 1 - \phi + \phi\frac{(\rho\beta_T)_s}{(\rho\beta_T)_f}, \\ f_4 &= \frac{k_s + 2k_f - 2\phi\left(k_f - k_s\right)}{k_s + 2k_f + \phi\left(k_f - k_s\right)}, \\ f_5 &= 1 - \phi + \phi\frac{\left(\rho c_p\right)_s}{\left(\rho c_p\right)_f}, \\ M &= \frac{\sigma_f B_0^2 d^2}{\rho_f \upsilon_f}, \\ Gr &= \frac{g\beta_{T\,f} d^2 (T_w - T_d)}{u_0 \upsilon_f}, \\ K &= \frac{K_0 N_0 d^2}{\rho_f \upsilon_f}, \\ H &= M + \lambda, \\ \Pr &= \frac{\mu_f c_{p_f}}{k_f}, \\ \lambda &= \frac{\beta d^2}{\upsilon_f}, \\ P_m &= \frac{K_0 d}{m u_0}. \end{aligned} \tag{11}$$

We now get the following the fractional parameter and CFD in equations (7) and (8), (9), respectively:

$${}^{CF}D_t^{\alpha} u(\xi,t) = \frac{f_2}{f_1}\frac{\partial^2 u(\xi,t)}{\partial\xi^2} - \frac{1}{f_1} H u(\xi,t) + \frac{1}{f_1} K(v(\xi,t) - u(\xi,t)) + \frac{f_3}{f_1} Gr\theta(\xi,t), \tag{12}$$

$$\frac{1}{P_m}\,{}^{CF}D_t^{\alpha} v(\xi,t) = u(\xi,t) - v(\xi,t), \tag{13}$$

$${}^{CF}D_t^{\alpha}\theta(\xi,t) = \frac{1}{\Pr}\frac{f_4}{f_5}\frac{\partial^2\theta(\xi,t)}{\partial\xi^2}, \tag{14}$$

where is the fractional parameter [35] and ${}^{CF}D_t^{\alpha}$ is the CF for the fractional operator:

$${}^{CF}D_t^{\alpha} f(t) = \frac{N(\alpha)}{(1-\alpha)}\int_0^t e^{\left(-\frac{\alpha(t-\tau)}{(1-\alpha)}\right)} f'(\tau) d(\tau). \tag{15}$$

Such that, $N(0) = N(1) = 1$, $\alpha \in (0,1)$

3. Solutions to the Problem

We get precise solutions to the system by combining the joint LT and FSFT.

3.1. Calculation of the Temperature Profile. Equation (14) Laplace transform yields the following results:

$$\frac{q n_0}{q + n_1}\frac{\Pr f_5}{f_4}\overline{\theta}(\xi,q) = \frac{\partial^2\theta(\xi,q)}{\partial\xi^2}. \tag{16}$$

Likewise, the converted version of equation (10) is as follows:

$$\left.\begin{aligned} &\overline{u}(\xi,q)\,|_{q=0} = \overline{v}(\xi,q)\,|_{q=0} = 0 \\ &\overline{\theta}(\xi,q)\,|_{q=0} = 0 \\ &\overline{u}(0,q)\,|_{y=0} = H(q), \overline{\theta}(0,q) = \frac{1}{q^2} \\ &\overline{u}(1,q) = 0, \overline{\theta}(1,q) = 0 \end{aligned}\right\}. \tag{17}$$

Multiplying equation (16) by $\mathrm{Sin}(n\pi)$ on both sides and then integrating it with y limits from 0 to d yields the following expression: Using starting and boundary conditions and then using the FSFT, we obtain:

$$\overline{\theta}_{\mathrm{FT}}(\eta,q) = \frac{Y_1}{q^2}\left(\frac{q + n_1}{q + Y_2}\right). \tag{18}$$

Equation (18) may also be expressed as follows:

$$\overline{\theta}_{FT}(\eta,q) = \frac{n_1 Y_1}{q^2 Y_2} - \frac{Y_1(n_1 - Y_2)}{q Y_2^2} + \frac{Y_1(n_1 - Y_2)}{Y_2^2(Y_2 + q)}. \tag{19}$$

Given is the inverse LT of equation (19).

$$\theta_{FT}(\xi,t) = \frac{n_1 Y_1}{Y_2}\, t - Y_3 + Y_3 \exp(-Y_2 t). \tag{20}$$

here,

$$\begin{aligned} n_0 &= \frac{1}{1-\alpha}, \\ n_1 &= \frac{\alpha}{1-\alpha}, \\ Y_1 &= \frac{n\pi}{\Pr f_5/f_4 n_0 + (n\pi)^2}, \\ Y_2 &= \frac{(n\pi)^2 n_1}{\Pr f_5/f_4 n_0 + (n\pi)^2}, \\ Y_3 &= \frac{Y_1(n_1 - Y_2)}{Y_2^2}, \end{aligned} \tag{21}$$

Equation using the inverse finite sine-Fourier transforms (20). We get the temperature profile's solution:

$$\theta(\xi,t) = (1-\xi)\,t + 2\sum_{n=1}^{\infty}\sin(n\pi\xi)\left(Y_3\left(1+\exp\left(-Y_2 t\right)\right)\right). \tag{22}$$

Equation (13)'s Laplace transform is used, together with equation (17), to provide the following results:

$$\frac{qn_0}{q+n_1}\overline{v}(\xi,q) = P_m\left(\overline{u}(\xi,q) - \overline{v}(\xi,q)\right). \tag{23}$$

As a consequence, following computation, we obtain

$$\overline{v}(\xi,q) = \left(\frac{q+n_1}{n_2(q+n_3)}\right)\overline{u}(\xi,q). \tag{24}$$

here,

$$n_2 = \frac{P_m + n_0}{P_m},$$
$$n_3 = \frac{n_1 P_m}{P_m + n_0}, \tag{25}$$

3.2. The Velocity Profile Solution. Taking use of the following transformation [23]:

$$u(\xi,t) = \overline{\chi}(\xi,t) + H(t)(1-\xi). \tag{26}$$

Equation (26) is applied to equation (12), and the solution is

$$\begin{aligned} {}^{CF}D_t^{\alpha}\left(\overline{\chi}(\xi,t) - (1-\xi)H(t)\right) &= \frac{f_2}{f_1}\frac{\partial^2}{\partial\xi^2}\left(\overline{\chi}(\xi,t) - (1-\xi)H(t)\right) + K\left(\frac{v(\xi,t)}{\left(\overline{\chi}(\xi,t) - (1-\xi)H(t)\right)} - 1\right), \\ &\cdot\frac{1}{f_1}\left(\overline{\chi}(\xi,t) - H(t)(1-\xi)\right) - H\left(\frac{1}{f_1}\overline{\chi}(\xi,t) - H(t)\frac{1}{f_1}(1-\xi)\right) + Gr\frac{f_3}{f_1}\theta(\xi,t). \end{aligned} \tag{27}$$

Ics and BCs with transformations are as follows:

$$\overline{\chi}(0,t) = \overline{\chi}(\xi,0) = \overline{\chi}(1,t) = 0. \tag{28}$$

Equations (27) and (28), when applied with the Laplace transform, result in

$$\frac{n_0 q}{q+n_1}\overline{\chi}(\xi,q) + \frac{n_0 q}{q+n_1}(1-\xi)H(q) = \left\{\begin{array}{c} \dfrac{f_2}{f_1}\dfrac{d^2}{d\xi^2}\overline{\chi}(\xi,q) + \dfrac{1}{f_1}K\left\{\left(\dfrac{q+n_1}{n_2(q+n_3)}\right) - 1\right\}\left(\overline{\chi}(\xi,q) + (1-\xi)H(q)\right) \\ -\dfrac{1}{f_1}H\overline{\chi}(\xi,q) - \dfrac{1}{f_1}H(1-\xi)H(q) + \dfrac{f_3}{f_1}Gr\overline{\theta}(\xi,q) \end{array}\right\}. \tag{29}$$

Next, we apply the finite sine Fourier transforms to equation (29) to obtain

$$\begin{aligned} \overline{\chi}_{\mathrm{FT}}(\xi,q) &= \left(\frac{q^2 - n_4 q - n_5}{q^2 + Y_4 q + Y_5}\right)(1-\xi)H(q) \\ &+ \frac{f_3}{f_1}\frac{Gr\,n_2 Y_1}{q^2}\cdot\frac{(q+n_1)^2}{q+Y_2}\cdot\frac{(q+n_3)}{q^2+Y_4 q+Y_5}. \end{aligned} \tag{30}$$

Equation (30) can be expressed as follows:

$$\begin{aligned} \overline{\chi}_{\mathrm{FT}}(y,q) &= \left\{\frac{Y_9}{q-Y_7} + 1 - \frac{Y_8}{q+Y_6}\right\}(1-y)H(q) \\ &- \left\{\frac{Y_{10}}{q^2} - \frac{Y_{11}}{q} - \frac{Y_{12}}{q+Y_2} - \frac{Y_{13}}{q+Y_6} - \frac{Y_{14}}{q-Y_7}\right\}, \end{aligned} \tag{31}$$

where

$$
\begin{aligned}
n_4 &= \frac{n_0 n_1 n_2 - H + K/f_1}{n_2\left(n_0 + H/f_1\right)},\\
n_5 &= \frac{K n_1 - H n_2 n_1 n_3}{f_1 n_2\left(n_0 + H/f_1\right)},\\
n_6 &= \frac{GrY_1 n_2 f_3}{f_1},\\
c_1 &= n_2\left(n_1 + n_3\right),\\
c_2 &= n_0 n_1 n_2,\\
c_3 &= n_1 n_2 n_3,\\
c_4 &= n_0 n_2 n_3,\\
c_5 &= n_1 n_4,\\
c_6 &= n_1 n_5 n_6,\\
c_7 &= n_0 n_2\\
Y_4 &= \frac{c_4 + (n\pi)^2 c_1 - n_1^2 K/f_1 - H\, c_1/f_1}{c_7 + (n\pi)^2 n_2 - K/f_1 - H\, n_2/f_1},\\
Y_5 &= \frac{(n\pi)^2 c_5 - c_6 K/f_1 - H/f_1\, c_5}{n_7 + (n\pi)^2 n_2 - K/f_1 - H/f_1\, n_2},\\
Y_6 &= \frac{Y_4 - \sqrt{Y_4^2 - 4Y_5}}{2},\\
Y_7 &= \frac{Y_4 + \sqrt{Y_4^2 - 4Y_5}}{2},\\
Y_8 &= \frac{n_4 + n_5 Y_6 - Y_6^2}{Y_6 + Y_7},\\
Y_9 &= \frac{Y_7^2 + n_5 Y_7 - n_4}{Y_6 + Y_7},\\
Y_{10} &= \frac{n_6 n_1^2 n_3}{Y_2 Y_6 Y_7},\\
Y_{11} &= \frac{n_6\left(n_1^2 n_3\left(Y_2 Y_7 - Y_2 Y_6 + Y_6 Y_7\right) - Y_2 Y_6 Y_7\left(n_1^2 + 2n_1 n_3\right)\right)}{\left(Y_2 Y_6 Y_7\right)^2},\\
Y_{12} &= \frac{n_6\left(n_1 n_3\left(n_1 - 2Y_1\right) + Y_2^2\left(n_3 - 2n_1 - 1\right) - n_1^2 Y_7\right)}{Y_2^2\left(Y_2 - Y_6\right)\left(Y_2 - Y_7\right)},\\
Y_{13} &= \frac{n_6\left(n_1 n_3\left(n_1 - 2Y_7\right) + Y_7^2\left(n_3 + 2n_1 - 1\right) - n_1^2 Y_6\right)}{Y_6^2\left(Y_6 - Y_2\right)\left(Y_6 + Y_7\right)},\\
Y_{14} &= \frac{n_6\left(n_1 n_3\left(n_1 + 2Y_7\right) + Y_7^2\left(n_3 + 2n_1 + 1\right) + n_1^2 Y_7\right)}{Y_7^2\left(Y_2 + Y_7\right)\left(Y_6 + Y_7\right)}.
\end{aligned}
\tag{32}
$$

Laplace inversion of equation (31), as

$$\overline{\chi}_{FT}(\xi,t)=\left\{\begin{array}{c}\{H(t)-H(t)*Y_8\exp(-Y_6t)+Y_9H(t)*\exp(Y_7t)\}(1-\xi)-Y_{10}t\\+Y_{11}+Y_{12}\exp(-Y_2t)+Y_{13}\exp(-Y_6t)+Y_{14}\exp(Y_7t)\end{array}\right\}. \tag{33}$$

Equation (33) is inverse FSFT, as follows:

$$\overline{\chi}(\xi,t)=2\sum_{n=1}^{\infty}\left(\begin{array}{c}\{H(t)-\exp(-Y_6t)Y_8*H(t)+\exp(tY_7)Y_9*H(t)\}(1-\xi)\\-Y_{10}t+Y_{11}+Y_{12}\exp(-Y_2t)+Y_{13}\exp(-Y_6t)+Y_{14}\exp(Y_7t)\end{array}\right)\sin(n\pi\xi). \tag{34}$$

The following is obtained from (26) using equation (34):

$$u(\xi,t)=H(t)(1-\xi)+2\sum_{n=1}^{\infty}\left(\begin{array}{c}\{H(t)-Y_8\exp(-Y_6t)*H(t)+Y_9\exp(Y_7t)*H(t)\}(1-\xi)\\-Y_{10}t+Y_{11}+Y_{12}\exp(-Y_2t)+Y_{13}\exp(-Y_6t)+Y_{14}\exp(Y_7t)\end{array}\right)\sin(n\pi\xi). \tag{35}$$

4. Special Case: Without Particle Velocities, the Brinkman Nanofluid Model Shows

When we put $v(y,t)=0$ into equation (8), we get a model for a fluid with a single phase of flow.

$$\begin{aligned}\frac{\partial u(\xi,t)}{\partial t}&=\frac{f_2}{f_1}\frac{\partial^2u(\xi,t)}{\partial\xi^2}-\frac{1}{f_1}Hu(\xi,t)\\&\quad-\frac{1}{f_1}K(u(\xi,t))+\frac{f_3}{f_1}Gr\theta(\xi,t).\end{aligned} \tag{36}$$

Putting equation (36) via its definition of fractional derivatives ${}^{CF}D_t^{\alpha}$, we get

$$\begin{aligned}{}^{CF}D_t^{\alpha}u(\xi,t)&=\frac{f_2}{f_1}\frac{\partial^2u(\xi,t)}{\partial\xi^2}-\frac{1}{f_1}K(u(\xi,t))\\&\quad-\frac{1}{f_1}Hu(\xi,t)+\frac{f_3}{f_1}Gr\theta(\xi,t).\end{aligned} \tag{37}$$

A Laplace transform applied to equation (37) ultimately yields:

$$\frac{n_0q}{q+n_1}\overline{\chi}(\xi,q)+\frac{n_0q}{q+n_1}(1-\xi)H(q)=\left\{\begin{array}{c}\frac{f_2}{f_1}\frac{d^2}{d\xi^2}\overline{\chi}(\xi,q)-\frac{1}{f_1}K(\overline{\chi}(\xi,q)+(1-\xi)H(q))\\-\frac{1}{f_1}H\overline{\chi}(\xi,q)-H(1-\xi)\frac{1}{f_1}H(q)+Gr\frac{f_3}{f_1}\overline{\theta}(\xi,q)\end{array}\right\}. \tag{38}$$

Transforming (38) into a function of its FSFT, we get

$$\overline{\chi}_{FT}(\xi,q)=\frac{n_8}{q^2}\cdot\frac{(q+n_1)}{(q+Y_2).(q+Y_{26})}-(1-\xi)H(q).\frac{(q+n_7)}{(q+Y_{26})}. \tag{39}$$

Using partial fraction w.r.t. s, we may decompose the right-hand side of equation (39), yielding:

$$\begin{aligned}\overline{\chi}_{FT}(\xi,q)&=\left(\frac{Y_{27}}{q}+\frac{Y_{28}}{q^2}+\frac{Y_{29}}{q+Y_1}+\frac{Y_{30}}{q+Y_{26}}\right)\\&\quad-\left\{1-\frac{Y_{26}-n_7}{q+Y_{26}}\right\}(1-\xi)H(q),\end{aligned} \tag{40}$$

where

$$Y_{26}=\frac{n_1f_2/f_1(n\pi)^2+n_1/f_1(K+H)}{n_0+f_2/f_1(n\pi)^2+1/f_1(K+H)},$$

$$n_7=\frac{n_1/f_1(K+H)}{n_0+1/f_1(K+H)},$$

$$n_8=\frac{f_3}{f_1}GrY_1,$$

$$Y_{27}=\frac{n_8Y_2-n_1n_8}{Y_2^2(Y_2-Y_{26})}+\frac{n_8Y_{26}-n_1n_8}{Y_{26}^2(Y_{26}-Y_1)},$$

$$Y_{28}=\frac{n_1n_8}{Y_1Y_{26}},$$

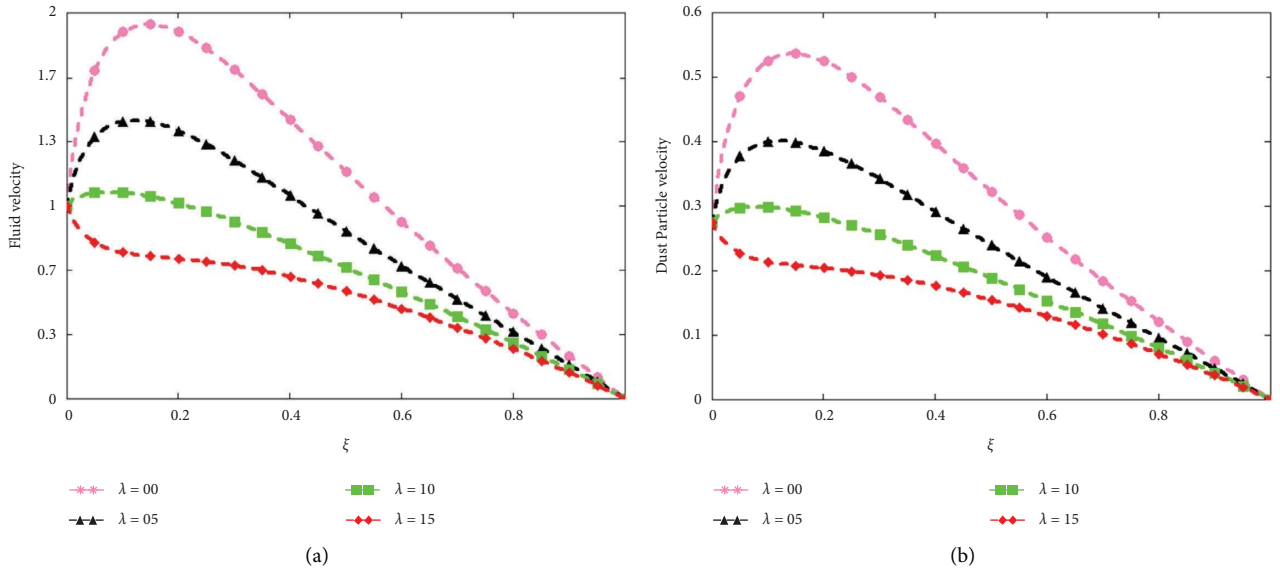

Figure 2: The effect of the Brinkman parameter on both velocities.

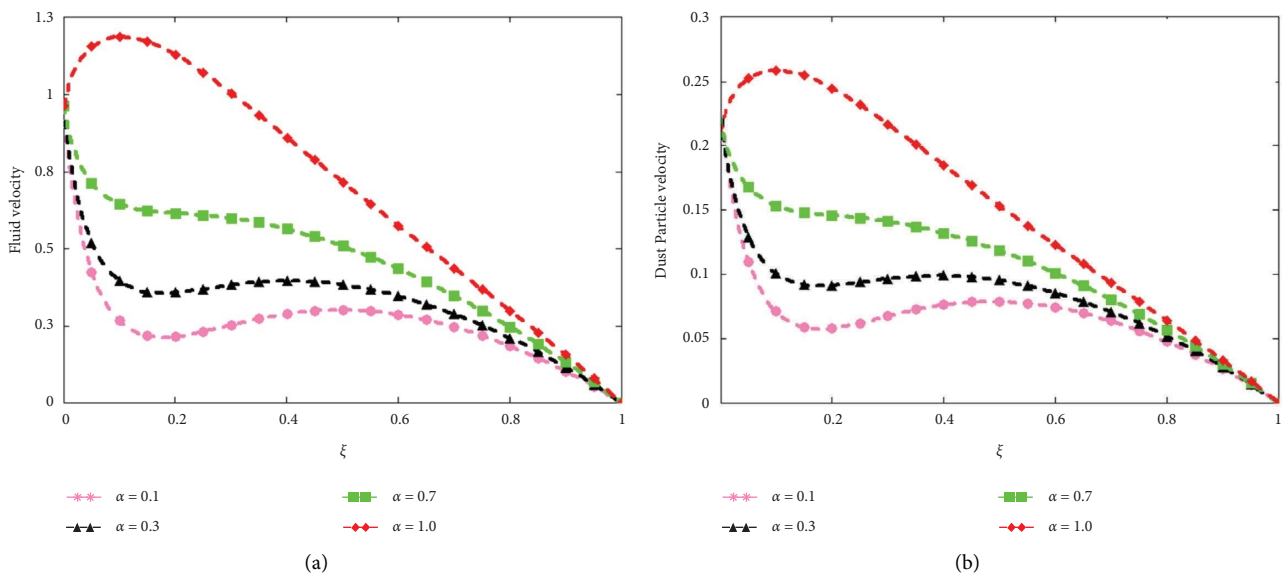

Figure 3: The effect of the fractional parameter on both velocities.

$$Y_{29} = \frac{n_1 n_8 - n_8 Y_2}{Y_2^2 (Y_2 + Y_{26})},$$
$$Y_{30} = \frac{n_1 n_8 - n_8 Y_{26}}{Y_{26}^2 (Y_1 + Y_{26})}. \tag{41}$$

To get (26), we substitute the inverse transform of (40) using the joint LT and FSFT:

$$u(\xi, t) = H(t)(1 - \xi) + 2 \sum_{n=1}^{\infty} \begin{pmatrix} \{Y_{27} + t\, Y_{28} + Y_{29} \exp(-t\, Y_1) + Y_{30} \exp(-t\, Y_{26})\} \\ -(1 - \xi)\{H(t) - (Y_{26} - n_7) \exp(-Y_{26}\, t) * H(t)\} \end{pmatrix} \sin(n\pi\xi). \tag{42}$$

4.1. Nusselt Number. Nusselt number is obtained from equation (22) by using the connection from Khan et al. [29].

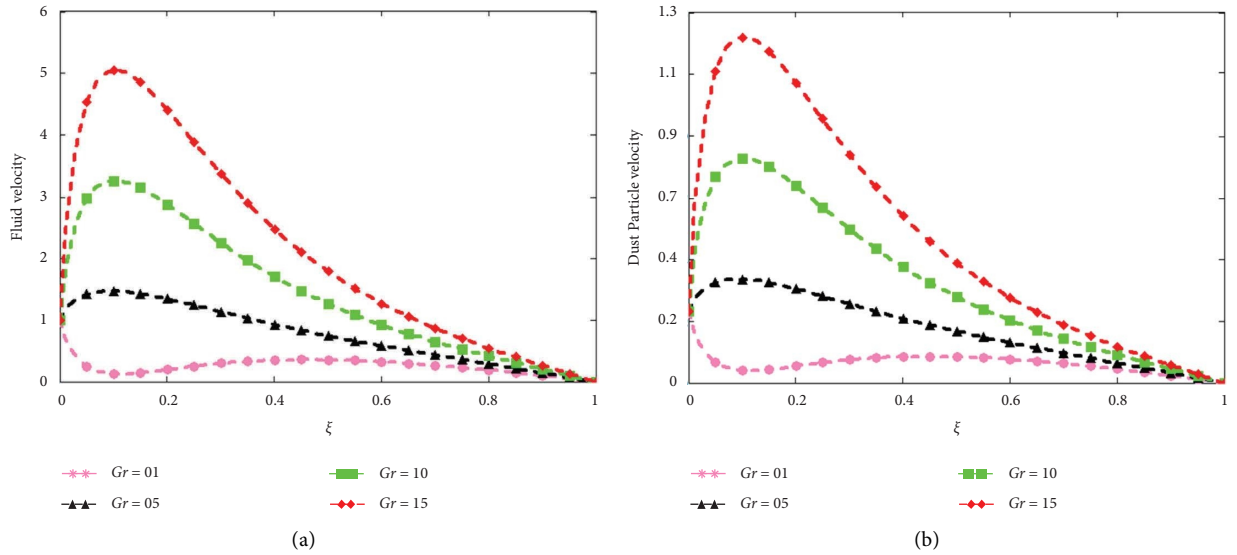

Figure 4: The effect of the Grashof number on both velocities.

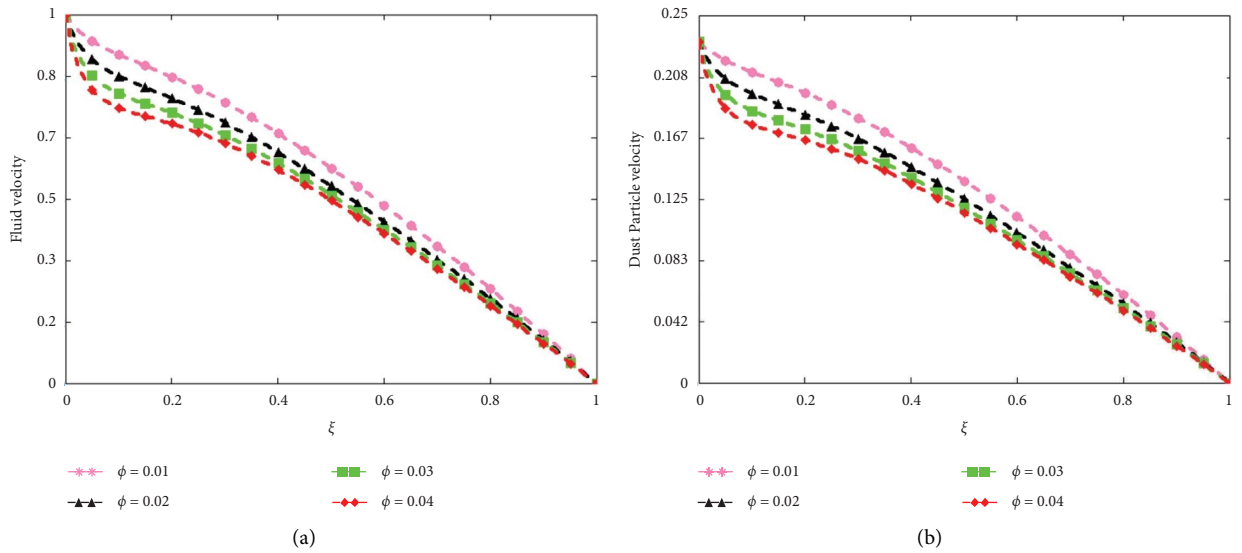

Figure 5: The effect of the volume fraction parameter on both velocities.

$$Cf = f_2 \frac{\partial u(\xi,t)}{\partial \xi}\bigg|_{\xi=0}, \qquad Nu = -f_4 \frac{\partial \theta(\xi,t)}{\partial \xi}\bigg|_{\xi=0}. \tag{43}$$

5. Results and Discussion

This article aims to investigate generalized Brinkman-type water–ethylene glycol (50 : 50) dusty nanofluids among microchannels that incorporate unsteady flow, heat transport, and MHD analysis. Combining Laplace and FSFT creates closed-form solutions. Figures and tables demonstrate how variables affect fluid and particle velocities and temperature.

Figures 2(a) and 2(b) show the study of the Brinkman parameter and contrast the velocities of Brinkman-type nanofluids and dust particles with those of Newtonian viscous fluids. When compared to a fluid of the Brinkman type $\lambda = 0$, a Newtonian viscous fluid has a high velocity. This illustrates that Brinkman parameter values delay velocity profiles more than Newtonian viscous fluids. Higher Brinkman values increase drag, slowing fluid and dust motion.

The effect of a fractional parameter α on the velocities of the Brinkman nanofluid and dusty fluid is examined in Figures 3(a) and 3(b). On both velocities, the memory effect is quite significant. When the other parameters are constant, changing the fractional parameter α leads to different solutions for the fluid and dust particle velocities. Which is a suitable option for experimental research so that the

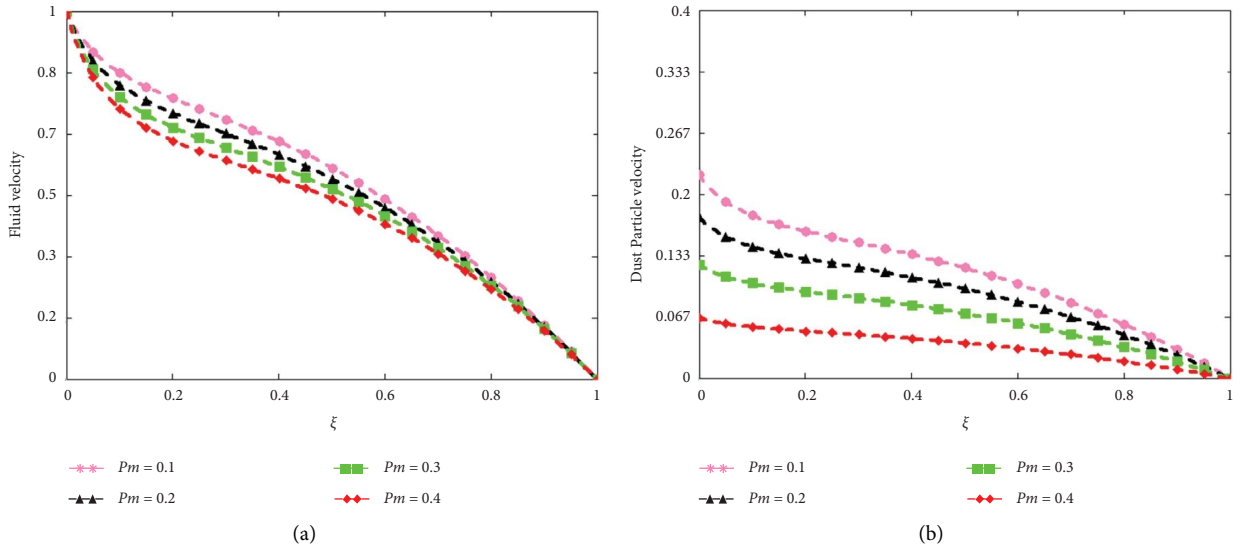

Figure 6: The effect of particle mass parameter on both velocities.

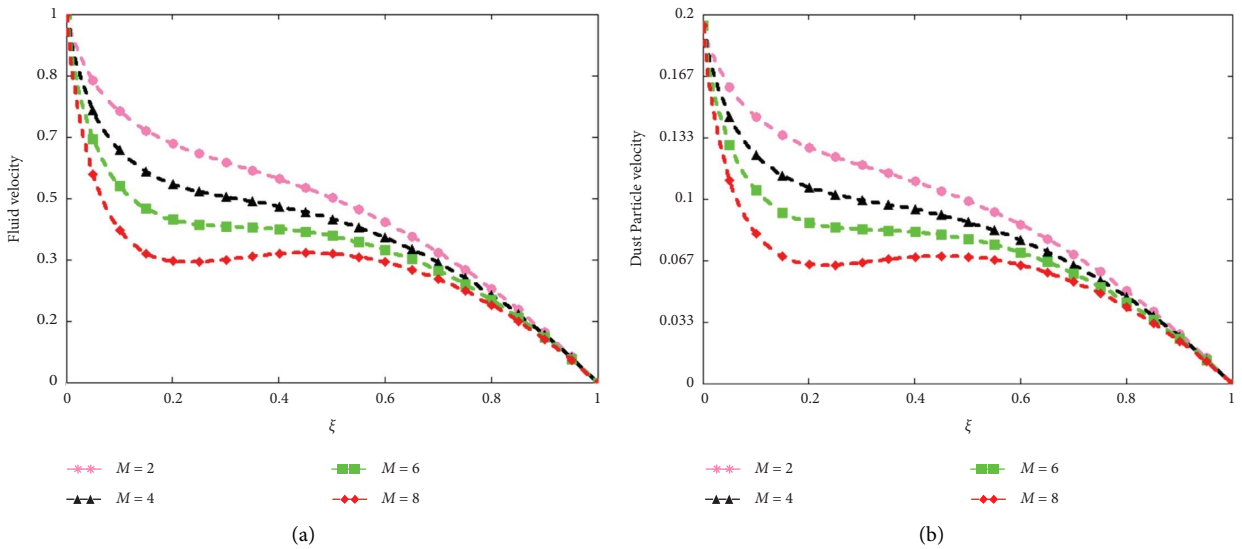

Figure 7: The effect of magnetic parameter on both velocities.

findings can be more accurately compared. The many solutions demonstrate that the fractional model is more plausible than the classical one.

The investigation of Gr on fluid and dust particle velocity is covered in Figures 4(a) and 4(b). Therefore, it is evident that as the Gr rises, so do the buoyant forces. Physically, the buoyant forces in the fluid, form in reaction to the greater temperature and quicken the fluid's velocity.

The impact of the volume fraction of fluid and dusty fluid on the velocities profile is seen in Figures 5(a), and 5(b). The velocity of the fluid decreases as its volume fraction increases, indicating that the nanoparticles are physically slowing the fluid's flow. The resistive forces that cause the nanoparticles to slow down in the channel were created when the fluid's nanoparticle concentration increased. The viscosity of the fluid rises with fluid concentration, decreasing both the fluid and dusty fluid velocities.

The results are shown as the impact of P_m on the velocities of Brinkman-type nanofluids and dust particles in Figures 6(a) and 6(b). Increased dust particle mass caused by rising P_m causes a slowdown in the flow of nanofluid and dust particle velocity. Physically, the fact is that, the fluid became more viscous with higher values of the mass particle parameter, which is why there is an apparent slowdown at both velocities.

Figures 7(a) and 7(b) illustrate how M affects the velocity of a nanofluid and dust particle. The viscosity of the momentum boundary layer contracts as M increases, increasing the Lorentz forces that are resistant to fluid flow and delaying the velocity of nanofluid and dust particles.

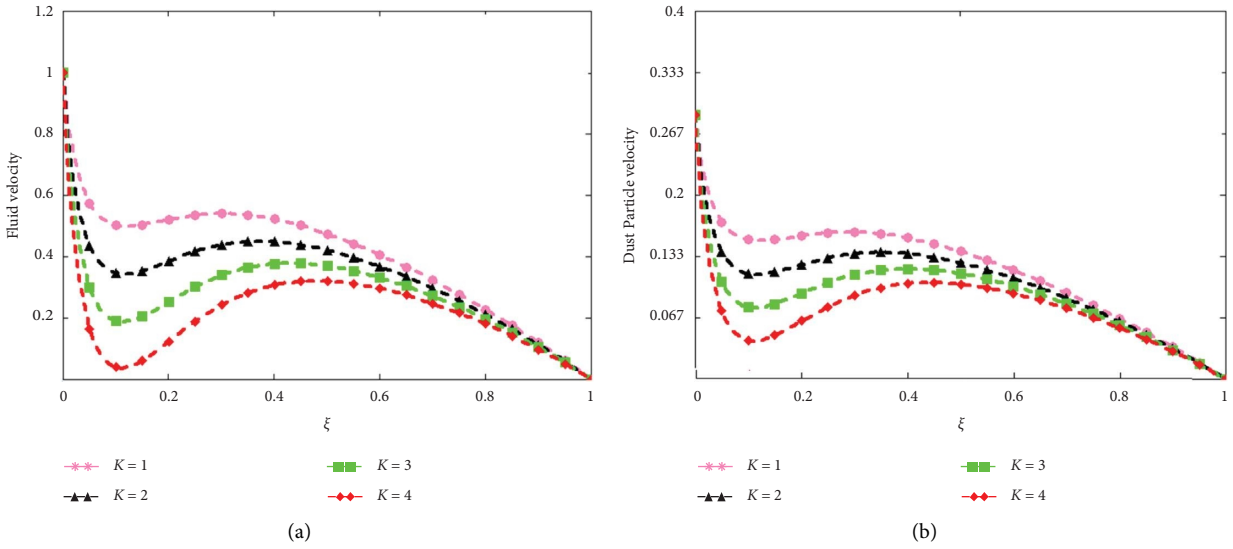

FIGURE 8: The effect of dusty fluid parameter on both velocities.

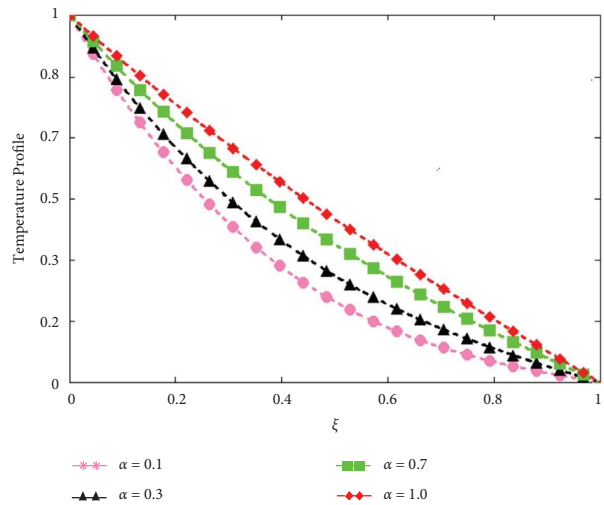

FIGURE 9: The consequence of fractional parameter on temperature.

It is clear that a rise in K would result in a delay in the viscous forces, which would increase fluid velocity, according to Stocks' drag formula ($k = 6\pi r\mu$) for sphere-shaped dust particles. As shown in Figures 8(a) and 8(b), increasing the amount of dust particles increases the nanofluid and dust particle velocities (b).

Figure 9 reports the effect of the fractional perimeter on the temperature profile. This, by fixing the other parameters, increases the generalization of the heat profile relative to the traditional one. Physically, this shows that the temperature profile may be made more realistic by altering the fractional parameter, which provides additional solutions.

The impacts of volume friction ϕ on $\theta(\xi, t)$ depicted in Figure 10. The range is between 0 and 0.04 when it reaches more than 0.04 segmentation occurs. A rise in the nanoparticle volume friction percentage will, in either scenario, result in a lower temperature as well as a change in the temperature distribution.

Table 1 displays the thermophysical characteristics of nanoparticles for your review. Table 2 shows the difference in skin friction caused by different parameter values. Skin friction is significant in several engineering areas, especially civil engineering. The viscous forces and, consequently, the surface friction increase as the λ and M raises. Skin friction is decreased by raising the Gr. By raising Gr the buoyancy forces to rise, the viscosity drops, and the surface friction goes down as a result. Table 2 clearly illustrates how skin friction reduces as volume friction ϕ increases.

Table 3 displays the Nusselt number against the volume fraction of nanofluid. It is clear that the enhancement of volume fractional makes the fluid more viscous, and as a result, the rate of heat transfer enhances up to 41.04478%.

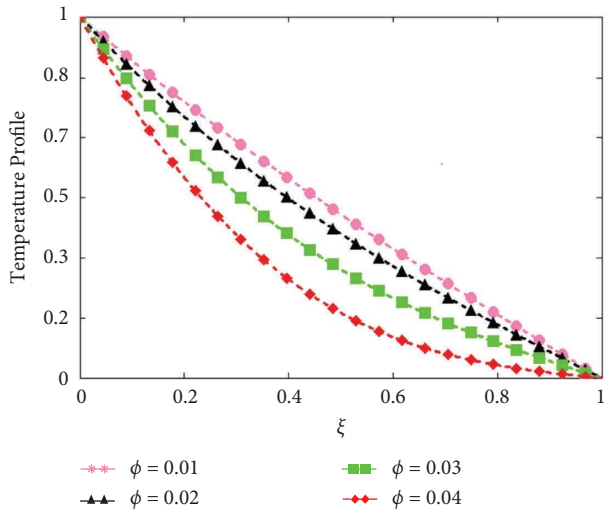

Figure 10: The consequence of the volume fraction parameter on temperature.

Table 1: Thermophysical properties.

Properties	Base fluids	Nanoparticles	
	Water–ethylene glycol	Cobalt ferrite	Magnetite
c_p (J/kg K)	3287	700	670
ρ (kg/m^3)	1057	4908	5180
σ (S/m)	0.005	1.1×10^7	0.74×10^6
K (W/m K)	0.424	3.6	9.8
Prandtl number, (Pr)	30	—	—

Table 2: The analysis of Cf.

t	α	λ	K	ϕ	Pm	M	Gr	Cf
0.5	0.6	1	4	0.02	0.4	5	10	**1.75**
0.5	**0.7**	1	4	0.02	0.4	5	10	**1.23**
0.5	0.6	**2**	4	0.02	0.4	5	10	**3.43**
0.5	0.6	1	**5**	0.02	0.4	5	10	**2.45**
0.5	0.6	1	4	**0.03**	0.4	5	10	**1.97**
0.5	0.6	1	4	0.02	**0.5**	5	10	**1.87**
0.5	0.6	1	4	0.02	0.4	**10**	10	**2.23**
0.5	0.6	1	4	0.02	0.4	**5**	**12**	**0.45**

The bold values represent the variation of each parameter.

Table 3: The analysis of Nu.

t	α	ϕ	Nu	%age
0.5	0.5	0.00	1.34	—
0.5	0.5	0.01	1.48	10.44776
0.5	0.5	0.02	1.61	20.14925
0.5	0.5	0.03	1.73	29.10448
0.5	0.5	0.04	1.89	41.04478

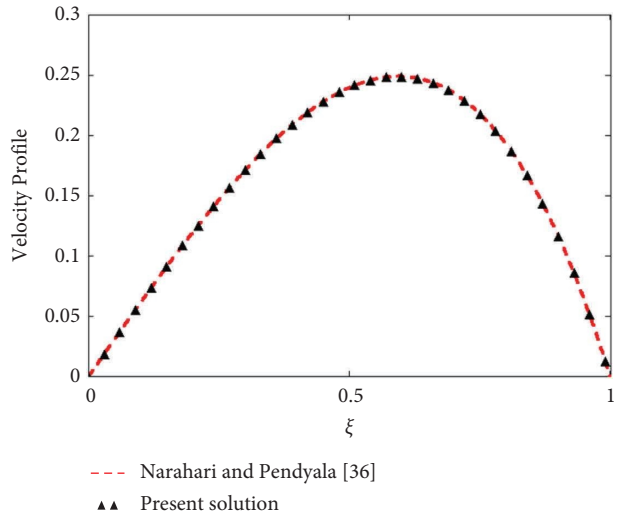

Figure 11: Comparative analysis of existing solutions with Narhari and Pendyala [36], when $P_m = K = M = \phi = 0, \alpha = 1$.

The comparison between the present study and that of Narahari and Pendyala [36] is shown in Figure 11, which demonstrates a high degree of congruence. The solutions are shown to be sound and valid, as each one precisely overlaps with the other.

6. Conclusions

In this study, the investigation of the generalized Brinkman-type dusty nanofluid at free convection temperature is the major focus. While the dust scatters evenly across the whole fluid, the flow is between the microchannels. Physical boundary conditions and PDE are used to formulate the issue. By combining the usage of the Laplace transform with the finite sine Fourier transform, the issue is generalized without a single kernel using Caputo–Fabrizio's fractional operator. The program Mathcad-15 is used to carry out parametric investigations. The validity and correctness of the present answers have been proven in several exceptional instances. The main findings from this study are as follows:

(i) Compared to the classical model, the fractional model of dusty nanofluid has a more realistic feature.

(ii) The variation of the fractional parameter α gets more realistic results for skin friction and heat transfer rate.

(iii) By combining Laplace transform and FSFT, we can reduce the computational time needed to obtain exact solutions for these types of problems.

(iv) The increase in Gr expands the nanofluid and particle velocities.

(v) The water–ethylene glycol nanofluids improve the heat transfer rate up to 41.04478%.

(vi) The findings of this study have practical applications in the engineering and product manufacturing industries. For example, dusty fluids are commonly used in gas cooling systems and nuclear reactors.

Nomenclature

$A \longrightarrow$: Variable temperature
T_d: Ambient temperature
t: Time
β_T: Coefficient of thermal epansion
B_0: Applied magnetic field
$u(\xi, t)$: Velocity of the nanofluid
u_0: Constant velocity
c_p: Specific heat capacity
Cf: Skin friction
$v(\xi, t)$: Velocity of the particle
CF: Caputo–Fabrizio
β: Nondimensional Brinkman fluid parameter
ρ: Density
d: Is the distance between parallel plates
Gr: Grashof number
μ: Dynamic viscosity
g: Gravitational acceleration
v: Kinematic viscosity
σ: Electrical conductivity
$H(t)$: Heaviside step function
α: Fractional parameter
K_0: Stock's resistance coefficient
K: Dusty fluid parameter
M: Nondimensional magnetic parameter
k: Thermal conductivity
θ: Dimensionless temperature of the fluid
$N(\alpha)$: Normalization function
N_0: Number density of the dust particles
Nu: Nusselt number
Pr: Prandtl number
P_m: Particles mass parameter
T: Temperature of the fluid

T_w: Temperature of wall
m: Mass of the particle
$(.)_{nf}$: Nanofluid
λ: Nondimensional Brinkman fluid
$(.)_f$: Fluid
$(.)_s$: Nanoparticle.

Data Availability

All the data in this study are available in the manuscript.

Conflicts of Interest

The authors declare that there are no conflicts of interest.

Authors' Contributions

Dolat khan was responsible for supervision, methodology, and draft writing, Musawa Yahay Almusawa was the project administrator and methodology. M. Ali Akbar was responsible for funding and draft writing. Waleed Hamali was responsible for the investigation, methodology, and draft writing.

References

[1] S. K. Das, N. Putra, P. Thiesen, and W. Roetzel, "Temperature dependence of thermal conductivity enhancement for nanofluids," *Journal of Heat Transfer*, vol. 125, no. 4, pp. 567–574, 2003.

[2] S. U. Choi and J. A. Eastman, *Enhancing thermal Conductivity of Fluids with nanoparticles(No. ANL/MSD/CP-84938; CONF-951135-29)*, Argonne National Lab (ANL), Argonne, IL, USA, 1995.

[3] V. Karthik, S. Sahoo, S. K. Pabi, and S. Ghosh, "On the phononic and electronic contribution to the enhanced thermal conductivity of water-based silver nanofluids," *International Journal of Thermal Sciences*, vol. 64, pp. 53–61, 2013.

[4] J. A. Eastman, S. U. S. Choi, S. Li, W. Yu, and L. J. Thompson, "Anomalously increased effective thermal conductivities of ethylene glycol-based nanofluids containing copper nanoparticles," *Applied Physics Letters*, vol. 78, no. 6, pp. 718–720, 2001.

[5] F. Rehman, M. I. Khan, M. Sadiq, and A. Malook, "MHD flow of carbon in micropolar nanofluid with convective heat transfer in the rotating frame," *Journal of Molecular Liquids*, vol. 231, pp. 353–363, 2017.

[6] M. Ijaz Khan, S. Ullah, T. Hayat, M. Waqas, M. Imran Khan, and A. Alsaedi, "Salient aspects of entropy generation optimization in mixed convection nanomaterial flow," *International Journal of Heat and Mass Transfer*, vol. 126, pp. 1337–1346, 2018.

[7] M. I. Khan, T. A. Khan, S. Qayyum, T. Hayat, M. I. Khan, and A. Alsaedi, "Entropy generation optimization and activation energy in nonlinear mixed convection flow of a tangent hyperbolic nanofluid," *The European Physical Journal Plus*, vol. 133, no. 8, pp. 329–420, 2018.

[8] D. Khan, P. Kumam, I. Khan, A. Khan, W. Watthayu, and M. Arif, "Scientific investigation of a fractional model based on hybrid nanofluids with heat generation and porous medium: applications in the drilling process," *Scientific Reports*, vol. 12, no. 1, pp. 6524–6613, 2022.

[9] K. Y. Leong, K. Ku Ahmad, H. C. Ong, M. J. Ghazali, and A. Baharum, "Synthesis and thermal conductivity characteristic of hybrid nanofluids–a review," *Renewable and Sustainable Energy Reviews*, vol. 75, pp. 868–878, 2017.

[10] D. Khan, P. Kumam, I. Khan, K. Sitthithakerngkiet, A. Khan, and G. Ali, "Unsteady rotating MHD flow of a second-grade hybrid nanofluid in a porous medium: Laplace and Sumudu transforms," *Heat Transfer*, vol. 51, no. 8, pp. 8065–8083, 2022.

[11] M. Saqib, I. Khan, and S. Shafie, "Application of fractional differential equations to heat transfer in hybrid nanofluid: modeling and solution via integral transforms," *Advances in Difference Equations*, vol. 2019, no. 1, pp. 52–18, 2019.

[12] B. Ross, "The development of fractional calculus 1695–1900," *Historia Mathematica*, vol. 4, no. 1, pp. 75–89, 1977.

[13] T. F. Nonnenmacher and R. Metzler, "On the Riemann-Liouville fractional calculus and some recent applications," *Fractals*, vol. 03, no. 03, pp. 557–566, 1995.

[14] S. Jiang, J. Zhang, Q. Zhang, and Z. Zhang, "Fast evaluation of the Caputo fractional derivative and its applications to fractional diffusion equations," *Communications in Computational Physics*, vol. 21, no. 3, pp. 650–678, 2017.

[15] M. M. Bhatti, M. B. Arain, A. Zeeshan, R. Ellahi, and M. H. Doranehgard, "Swimming of Gyrotactic Microorganism in MHD Williamson nanofluid flow between rotating circular plates embedded in porous medium: application of thermal energy storage," *Journal of Energy Storage*, vol. 45, Article ID 103511, 2022.

[16] M. I. Khan, M. Waqas, T. Hayat, M. I. Khan, and A. Alsaedi, "Chemically reactive flow of upper-convected Maxwell fluid with Cattaneo–Christov heat flux model," *Journal of the Brazilian Society of Mechanical Sciences and Engineering*, vol. 39, no. 11, pp. 4571–4578, 2017.

[17] M. Caputo, "Linear models of dissipation whose Q is almost frequency independent—II," *Geophysical Journal International*, vol. 13, no. 5, pp. 529–539, 1967.

[18] E. F. Doungmo Goufo, "Application of the caputo-fabrizio fractional derivative without singular kernel to korteweg-de Vries-burgers equation," *Mathematical Modelling and Analysis*, vol. 21, no. 2, pp. 188–198, 2016.

[19] M. Caputo and M. Fabrizio, "A new definition of fractional derivative without singular kernel," *Progress in Fractional Differentiation and Applications*, vol. 1, no. 2, pp. 1–13, 2015.

[20] M. Caputo and M. Fabrizio, "Applications of new time and spatial fractional derivatives with exponential kernels," *Progress in Fractional Differentiation and Applications*, vol. 2, no. 1, pp. 1–11, 2016.

[21] A. Atangana and E. F. Doungmo Goufo, "The Caputo-Fabrizio fractional derivative applied to a singular perturbation problem," *International Journal of Mathematical Modelling and Numerical Optimisation*, vol. 9, no. 3, pp. 241–253, 2019.

[22] P. Verma and M. Kumar, "Analysis of a novel coronavirus (2019-nCOV) system with variable Caputo-Fabrizio fractional order," *Chaos, Solitons & Fractals*, vol. 142, Article ID 110451, 2021.

[23] H. Mohammadi, S. Kumar, S. Rezapour, and S. Etemad, "A theoretical study of the Caputo–Fabrizio fractional modeling for hearing loss due to Mumps virus with optimal control," *Chaos, Solitons & Fractals*, vol. 144, Article ID 110668, 2021.

[24] B. Mahanthesh, "Hall effect on two-phase laminar boundary layer flow of dusty liquid due to stretching of an elastic flat sheet," *Mapana Journal of Sciences*, vol. 16, no. 3, pp. 13–26, 2017.

[25] H. C. Brinkman, "On the permeability of media consisting of closely packed porous particles," *Flow, Turbulence and Combustion*, vol. 1, no. 1, pp. 81–86, 1949.
[26] Y. Liu, S. Xiao, and Y. Lin, "Continuous dependence for the Brinkman–Forchheimer fluid interfacing with a Darcy fluid in a bounded domain," *Mathematics and Computers in Simulation*, vol. 150, pp. 66–82, 2018.
[27] M. Ramzan, Z. Un Nisa, M. Ahmad, and M. Nazar, "Flow of Brinkman fluid with heat generation and chemical reaction," *Complexity*, vol. 2021, Article ID 5757991, 11 pages, 2021.
[28] A. Kumar, R. Singh, G. S. Seth, and R. Tripathi, "Double diffusive magnetohydrodynamic natural convection flow of brinkman type nanofluid with diffusion-thermo and chemical reaction effects," *Journal of Nanofluids*, vol. 7, no. 2, pp. 338–349, 2018.
[29] A. Khan, D. Khan, I. Khan, F. Ali, F. U. Karim, and K. S. Nisar, "MHD flow of brinkman type H_2O-Cu, Ag, TiO_2 and Al_2O_3 nanofluids with chemical reaction and heat generation effects in a porous medium," *Journal of Magnetics*, vol. 24, no. 2, pp. 262–270, 2019.
[30] R. Dubey and P. V. S. N. Murthy, "The onset of double-diffusive convection in a Brinkman porous layer with convective thermal boundary conditions," *AIP Advances*, vol. 9, no. 4, Article ID 045322, 2019.
[31] P. Kumar and H. Mohan, "Double-diffusive convection in compressible viscoelastic dusty fluid through brinkman porous media," *American Journal of Fluid Dynamics*, vol. 2, no. 2, pp. 1–6, 2012.
[32] P. G. Saffman, "On the stability of laminar flow of a dusty gas," *Journal of Fluid Mechanics*, vol. 13, no. 1, pp. 120–128, 1962.
[33] K. M. Chakrabarti, "Note on boundary layer in a dusty gas," *AIAA Journal*, vol. 12, no. 8, pp. 1136-1137, 1974.
[34] P. K. Shukla and L. Stenflo, "Transverse shear waves generating vortex-like dust fluid motions in strongly coupled dusty plasmas," *Physics Letters A*, vol. 315, no. 3-4, pp. 244–247, 2003.
[35] D. Khan, S. Ullah, P. Kumam, W. Watthayu, Z. Ullah, and A. M. Galal, "A generalized dusty Brinkman type fluid of MHD free convection two phase flow between parallel plates," *Physics Letters A*, vol. 450, Article ID 128368, 2022.
[36] M. Narahari and R. Pendyala, "Exact solution of the unsteady natural convective radiating gas flow in a vertical channel," in *Proceedings of the AIP Conference Proceedings*, no. 1, pp. 121–124, American Institute of Physics, Park, Maryland, USA, September 2013.